Available online at www.sciencedirect.com
ScienceDirect
Catalysis Today 130 (2008) 149–159
CATALYSIS TODAY
www.elsevier.com/locate/cattod

Optimal promoter edge decoration of CoMoS catalysts: A combined theoretical and experimental study

A.D. Gandubert [a], E. Krebs [b], C. Legens [a], D. Costa [b,c,1], D. Guillaume [a], P. Raybaud [b,*]

[a] *IFP-Lyon, BP 3-69390 Vernaison, France*
[b] *IFP, 1 & 4 Avenue de Bois-Préau, 92852 Rueil-Malmaison Cedex, France*
[c] *Laboratoire de Réactivité de Surface - UMR 7609 CNRS, Université Pierre et Marie Curie, 4 Place Jussieu, 75252 Paris Cedex 05, France*

Available online 10 August 2007

Abstract

The present work combines X-ray Photoelectron Spectroscopy (XPS), catalytic tests, and density functional theory (DFT) modeling for determining the optimized Co edge decoration according to the stability and reactivity of the CoMoS active phase. Using the phase diagram and morphology of the CoMoS nano-crystallites determined by DFT calculations [Krebs et al. Catal. Today, this issue], the values of the Co/Mo ratio and the number of mixed Co–Mo sites are evaluated. DFT calculations of the 2p core level shift of Co at the edges with respect to the Co_9S_8 phase are compatible with the experimental positive binding energy shift measured by XPS on CoMoS catalysts. Moreover, the decomposition of the XPS spectral envelope is used to quantify the proportion of CoMoS phase and to normalize the catalytic activity in toluene-hydrogenation per edge site as a function of the Co/Mo ratio. The optimal Co/Mo ratio for the catalytic activity is found to reflect the presence of mixed Co–Mo sites at Mo-edge when considering the measured average size of particles and the calculated morphology. These results are helpful for an improved optimization of the promoter content in the CoMoS phase.

Keywords: Hydrotreatment; CoMoS; XPS; Density functional theory (DFT); Core level shift; Active sites; Volcano curve

1. Introduction

The production of ever cleaner fuels with low or even ultra low sulfur content, requires a continuous improvement of the catalytic materials used in the refinement industry. Especially, sulfides catalysts such as γ-alumina supported Co(Ni)MoS are widely used in hydrotreatment processes. The active phase of the industrial catalysts is made of a Co(Ni) promoted MoS_2 nano-crystallites and is at the core of many research investigations. Among these, X-ray photoelectron spectroscopy (XPS) is a widely used experimental technique to characterize and control the sulfided state of the catalyst. This technique is also very instructive to identify the electronic state of Co species [1–4] and Ni species [5–7] in the active phase and to quantify them [8]. More recently, density functional theory (DFT) appears as an efficient method to bring new insights on the local structure and electronic properties of the active phase [9]. In particular, the localization of the promoter at the edges of the MoS_2 nano-crystallites and their impact on the reactivity was the subject of fruitful investigations enabling a more precise description of the active sites [10–12]. Moreover, in line with the geometrical model earlier proposed by Kasztelan et al. [13], the stable morphology of the active phase in reaction conditions has been solved by DFT calculations [14–16]. In the present work, we focus on the CoMoS active phase investigated by a multitechnique approach combining X-ray photoelectron spectroscopy (XPS), transmission electron microscopy (TEM), catalytic tests and density functional theory (DFT) calculations. Our goal is thus to obtain a better determination of the optimal promoter decoration at the edges of the MoS_2 crystallites taking into account the crystallites' morphology effects.

In the next section, the experimental and theoretical methodologies are described. In Section 3, the XPS and

* Corresponding author. Tel.: +33 1 47 52 71 84; fax: +33 1 47 52 70 58.
E-mail address: pascal.raybaud@ifp.fr (P. Raybaud).
[1] Present address: Laboratoire de Physicochimie des surfaces - UMR 7045 CNRS, Ecole Nationale Supérieure de Chimie de Paris, 11 rue Pierre et Marie Curie, 75231 Paris Cedex, France.

0920-5861/$ – see front matter © 2007 Elsevier B.V. All rights reserved.
doi:10.1016/j.cattod.2007.06.041

Table 1
Definition and composition of the oxide catalysts

Catalyst	Mo loading (wt%)	Co loading (wt%)	P loading (wt%)	Co/Mo atomic ratio (theo.)	Co/Mo atomic ratio (exp.)
CoMoP(0.1)	14.3	0.9	2.6	0.1	0.09
CoMoP(0.2)	14.3	1.7	2.6	0.2	0.19
CoMoP(0.3)	14.3	2.6	2.6	0.3	0.30
CoMoP(0.4)	14.3	3.6	2.6	0.4	0.41
CoMoP(0.5)	14.3	4.6	2.6	0.5	0.47
CoMoP(0.6)	14.3	5.3	2.6	0.6	0.60
CoMoP(0.7)	14.3	6.1	2.6	0.7	0.68
MoP	14.3	–	2.6	–	–
Co	–	4.6	–	–	–

Theo., theoretical value and exp., experimental value obtained with X-ray fluorescence.

DFT results are presented. Finally, we make a proposal deduced from these two techniques for the most coherent model of morphology and active sites of the CoMoS phase. It will be shown how the concept of mixed edge site provides an interpretation of the activity in toluene-hydrogenation as a function of promoter content.

2. Methods

2.1. Experiments

2.1.1. Catalyst preparation

The oxidic precursors were prepared by incipient wetness impregnation of γ-alumina extrudates (from Axens) with impregnation solutions containing the appropriate amount of metal to be deposited. The impregnated extrudates were then placed in water-saturated atmosphere for at least 3 h and then dried at 120 °C overnight. Finally the solids were calcined under air at 500 °C during 2 h. The bimetallic CoMoP-type catalysts with various Co/Mo ratio were prepared with impregnation solutions of heteropolycompounds $P_2Mo_5O_{23}(-Co_x)$ obtained by dissolving molybdenum oxide –MoO_3– and cobalt hydroxide –$Co(OH)_2$– in a phosphoric acid aqueous solution [17]. A large excess of phosphoric acid, corresponding to 2.6 wt% P loading, was necessary to well dissolve the molybdenum and cobalt precursors. The Mo loading was of 14 wt% as Mo, the concentration of Co was adjusted to obtain various Co/Mo atomic ratio. These oxidic catalysts will be referred to as CoMoP(*X*), where *X* represents the Co/Mo atomic ratio. The Co loadings correspond to 0.9, 1.7, 2.6, 3.6, 4.6, 5.3 and 6.1 wt% Co for, respectively, 0.1, 0.2, 0.3, 0.4, 0.5, 0.6 and 0.7 ratio.

Two monometallic samples, prepared according the same method, were used as references for XPS spectra interpretations: one containing only cobalt and one composed of molybdenum doped by phosphorus. The impregnation solutions were prepared by dissolving cobalt hydroxide $Co(OH)_2$ in a sulfuric acid aqueous solution and molybdenum oxide MoO_3 in a phosphoric acid aqueous solution, for, respectively, the Co and MoP type catalysts that will be hereafter referred to as Co and MoP. The metal loadings were 4.6 wt% as Co for the Co sample and 14 wt% as Mo for the MoP solids. For each sample, the nomenclature, the theoretical composition and the atomic ratio are listed in Table 1. The comparison between theoretical and experimental ratio determined by X-ray fluorescence technique confirms the synthesis of the desired catalysts.

2.1.2. Sulfidation conditions

The oxide precursors were sulfided at atmospheric pressure under a H_2S/H_2 mixture with a $p(H_2S)/p(H_2)$ ratio about 0.17 and a gas flow of 2 L/h/g of catalyst. The samples were heated under the sulfiding mixture at a rate of 5 °C/min up to 400 °C and maintained at this temperature for 2 h. They were then cooled down to room temperature at a rate of 20 °C/min also under the reactive mixture. The sulfided catalysts were transferred into glass vials under vacuum in order to avoid any contact with air. The nomenclature of the sulfided samples will be the same as the oxidic one with the supplementary extension—*S*. The oxide references were sulfided as well.

2.1.3. TEM analysis

The sulfided samples were analyzed by TEM to determine the average length and stacking of the MoS_2 slabs by counting at least 350 particles. The extrudates were crushed into a fine powder, a small amount of which being ultra sonically diluted in ethanol. Two drops of this solution were deposited on a carbon-coated Cu grid and the solvent was evaporated under infrared light. TEM images were taken using a 200 kV JEOL-2010 transmission electron microscope equipped with a digital camera. All the sulfided samples with the different Co/Mo ratio showed a similar slab morphology with a mean length around 3.3 ± 0.2 nm and an average stacking of 1.9.

2.1.4. XPS analysis

The XPS sampling of the sulfided catalysts was performed in a glove box under argon atmosphere, with controlled oxygen and water level (less than 20 ppm) in order to avoid their partial reoxidation. The samples were crushed and pressed onto an indium foil that was attached to the sample holder via a double side carbon tape. The sample holder was then moved directly to the introduction chamber of the XPS spectrometer, thanks to the special connection of the glove box to the XPS spectrometer. The XPS spectra were recorded on a Kratos Axis Ultra instrument with Al monochromator source (1486.6 eV) and a hemi-spherical analyzer operating at fixed pass energy of 40 eV. The measurements were made at ambient temperature in

steps of 0.05 eV for cobalt, 0.1 eV for sulfur and 0.1 eV for molybdenum, and at a pressure lower than 1×10^{-6} Pa in the sample analysis chamber. Binding energies (BE) of the various elements have been referenced to the C 1s level of the contamination carbon at 284.6 eV. The curves were integrated applying a Shirley type baseline. The collected spectra were analyzed by using CasaXPS software, Version 2.0.71. The decomposition of the S 2p, Mo 3d and Co 2p XPS spectra were performed using the appropriate oxide and sulfided references as supported monometallic catalysts defined before and led us to propose a protocol to quantify inter alia the CoMoS phase [3,8]. The effective atomic concentration [i] of the atom i was obtained from the measurement of the corresponding total peak area Ai and the use of appropriate sensitivity factor Si furnished by the constructor. To approach the effective atomic surface concentrations, all the atoms (except the contamination carbon) detected on the surface were taken into account in Eq. (1).

$$[i] = \frac{Ai/Si}{\sum_{i=1}^{i=n}(Ai/Si)} \quad (1)$$

For one atom, the signal obtained can be decomposed into different contributions relative to various chemical species. The calculation of the respective contribution of each peak area will lead to the knowledge of the relative proportion of each chemical form for a given atom. For example in the case of Co atoms detected as Co(II), CoMoS and Co_9S_8, the relative amount in CoMoS phase is given by Eq. (2) [8].

$$\%\mathrm{CoMoS} = \frac{A_{\mathrm{CoMoS}}}{A_{\mathrm{CoMoS}} + A_{\mathrm{Co(II)}} + A_{\mathrm{Co_9S_8}}} \times 100 \quad (2)$$

with A_{CoMoS}, $A_{\mathrm{Co(II)}}$ and $A_{\mathrm{Co_9S_8}}$ the experimental XPS area of, respectively, CoMoS, Co(II) and Co_9S_8 species.

We can then deduce the effective amount of CoMoS phase noted [CoMoS] by multiplying the relative value with the total Co content (3).

$$[\mathrm{CoMoS}] = \%\mathrm{CoMoS} \cdot [\mathrm{Co}]/100 \quad (3)$$

Two samples have been analyzed for each catalyst and the data presented correspond to the average values of the two analysis. The estimated error is evaluated to 7% absolute for Co and in the form $ax + b$ for Mo with $a = 0.04$ and $b = 0.42$.

2.1.5. Catalytic measurements

The catalytic performances of the samples in toluene-hydrogenation are evaluated in hydrotreatment conditions. The catalytic tests were carried out in a fixed bed high pressure flow microreactor under the following conditions: 2 cm^3 of crushed extrudates (300–1000 μm) diluted in SiC, a total pressure of 60 bar corresponding to $p(H_2S) = 2.15$ bar, $p(H_2) = 36.9$ bar, reaction temperature of 350 °C, liquid hourly space velocity (LHSV) of 2 h^{-1}, hydrogen-to-feed ratio of 450 L/L. The feed consists of dimethyldisulfide (5.9 wt%) and toluene (20 wt%) mixture in cyclohexane. After the unit was pressure tested at room temperature, the temperature was increased at 3 °C/min to 350 °C. Steady-state conversion was measured after 2 h on stream. Reaction products were analyzed by on line gas chromatography. The activity in toluene-hydrogenation was expressed considering a first-order reaction.

2.2. DFT calculations

2.2.1. Surface energy and morphology determination

The DFT results used in this paper are presented in details in the companion paper by Krebs et al. published in this issue [16]. For sake of clarity, we only report the main insights resulting from this study. All total energy calculations are based on the plane wave density functional theory within the generalized gradient approximation [18,19] and periodic boundary conditions. In a consistent way with our previous works [14], we used the Vienna ab initio simulation package to solve the Kohn–Sham equations [20] within the projected augmented wave (PAW) formalism [21]. All details on the methodology (approximations, cut-off energy, convergence criteria, cell's size) are reported in [16], where it has been explored the various possible locations and structures for the Co atoms at the two edges (so called S-edge and M-edge) of the CoMoS nano-crystallites. Moreover, this theoretical study explains how the equilibrium Gibbs Curie Wulff morphologies of the CoMoS nano-crystallite is determined as a function of the Co promoter edge content and of the reaction conditions by calculating the energy of the M-edge and S-edge. The variable representing the reaction conditions ($p(H_2S)/p(H_2)$ and T) is the chemical potential of sulfur, $\Delta\mu_S$. In the present work, the $\Delta\mu_S$ value corresponding to $p(H_2S)/p(H_2)$ and T used in the sulfidation conditions and reaction conditions (Section 2.1) is close to −0.87 eV.

2.2.2. Core level shift

To calculate the binding energy (BE) of core electrons using DFT, two approximations can be made. In the "initial state approximation", it is assumed that the binding energy of the core electron is directly related to the energy level of its core orbital, $\varepsilon_c(n_c)$, following the Koopman's theorem [22]. In the "final state approximation", one must calculate the energy difference between two distinct states:

$$\mathrm{BE} = E(n_c - 1) - E(n_c) \quad (4)$$

$E(n_c)$ is the energy of the unexcited ground state, and $E(n_c - 1)$ is the energy of the excited state where one electron is transferred from the core level of one particular atom (n_c) to the valence band. For such DFT calculation, we take advantage of the PAW formalism implemented in VASP because such an all electron method with frozen core approximation also allows the generation of the corresponding core excited ionic potential during the calculations. Following the so-called "$(Z + 1)$ approximation", the core hole ($n_c - 1$) is modeled by adding one nuclear charge to the core atom and simultaneously one valence electron [23,24]. Hence, the screening by other valence electrons is included, whereas the screening by the core electrons is not taken into account. Actually, the difference given by Eq. (5) can be obtained using the Slater–Janak theorem [25,26]:

$$\mathrm{BE} = E(n_c - 1) - E(n_c) \approx -\varepsilon_c\left(n_c - \frac{1}{2}\right) \quad (5)$$

$\varepsilon_c(n_c - (1/2))$ is the Kohn–Sham eigenvalues of the given core level with an occupation decreased by half an electron. This approach corresponds to the final state approximation used in the current study. However, the absolute value of $\varepsilon_c(n_c - (1/2))$ cannot be directly compared to experimental values (according to different reference energies in experiment and theory). As a consequence, only binding energy differences, ΔBE, for core states of the given atom in two different environments, are relevant for a comparison with data obtained from XPS analysis.

For instance, to determine the variation of the binding energies for the 2p core levels of Co in CoMoS and Co_9S_8, calculations are done using the 2p core level of sulfur as references in both systems. This approach is comparable to the experimental one used in XPS analysis. For the CoMoS slab, the BE difference between the 2p core level of Co and the 2p core level of sulfur atoms belonging to the MoS_2 bulk part of the CoMoS slab, is:

$$\Delta BE(Co{-}S|_{CoMoS}) = -\varepsilon_{Co/CoMoS}\left(n_c - \frac{1}{2}\right) + \varepsilon_{S_{bulk}/CoMoS}\left(n_c - \frac{1}{2}\right) \quad (6)$$

For the Co_9S_8 bulk phase, the corresponding binding energy differences:

$$\Delta BE(Co{-}S|_{Co_9S_8}) = -\varepsilon_{Co/Co_9S_8}\left(n_c - \frac{1}{2}\right) + \varepsilon_{S/Co_9S_8}\left(n_c - \frac{1}{2}\right) \quad (7)$$

From Eqs. (6) and (7), we thus deduce the ''edge core level shift'' (ECLS) between the Co 2p electrons in the CoMoS phase and in the Co_9S_8 bulk sulfide:

$$ECLS = \Delta BE(Co{-}S|_{CoMoS}) - \Delta BE(Co{-}S|_{Co_9S_8}) \quad (8)$$

Some caution must be taken for the periodic supercell size used for the calculation of the $-\varepsilon_c(n_c - (1/2))$ value. To investigate the excited core located on one isolated (Co or S) atom in the 3D periodic cell without artificially exciting a too high concentration of core level located on equivalent atoms in the cell, the size of the supercell for the CoMoS slab contains 4 non-equivalent edge atoms and is enlarged to 7 metal layers in the direction perpendicular to the edge. In particular, this size ensures that the excited S atom in the middle of the CoMoS slab is an electronic state very close to bulk MoS_2 and that the excited Co atom at the edge is isolated from the next one by 3 neighboring metal edge atoms.

3. Results and discussion

3.1. XPS characterization

3.1.1. Mo-species

The Mo 3d spectrum for the CoMoP(0.3)-S sulfided catalyst is presented in Fig. 1 and decomposed according to a previous detailed work into different chemical species [8,27]. Three different oxidation degrees (VI), (V) and (IV), respectively,

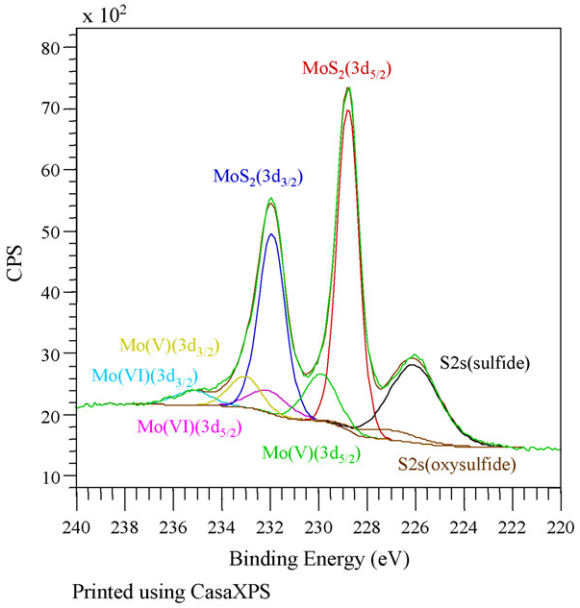

Fig. 1. Decomposition of Mo 3d XPS spectrum for CoMoP(0.3)-S catalyst.

attributed to oxide, oxysulfide and sulfide phases are reported and highlight the majority amount of MoS_2 phase which can be quantify from the respective measured areas. S 2s contributions are reported but not taken into account in the quantification. The same decomposition procedure was applied to the set of sulfided samples and lead to similar results, which is not surprising as the sulfiding conditions and Mo content are the same for all the catalysts. The binding energy of the main contributions are reported in Table 2 and are in good agreement with values reported in the literature [28–30].

3.1.2. Co-species

Fig. 2 shows the superimposition of the oxide CoMoP(0.3) and the sulfided CoMoP(0.3)-S and monometallic Co-S samples supported on alumina. We clearly observe that the main Co $2p_{3/2}$ contribution varies in binding energy position according to the oxidation/sulfidation state of the sample and to the presence of Mo atoms.

The procedure used to decompose and identify the different Co species will not be detailed here as it has already been reported in [8]. However, we notice that after sulfidation Co is present as surface cobalt oxide Co(II), mixed phase CoMoS and sulfided Co_9S_8. The formation of the Co_9S_8 phase was also observed by Mössbauer Emission Spectroscopy study of CoMo/C catalysts [31]. These species are evidenced, respectively, to the binding energy of the main Co $2p_{3/2}$ core level, even if the position between the two sulfided Co species differs only to 0.55 eV which is the limit of resolution in the experimental conditions. So it is necessary, to distinguish the two forms, to apply restrictive constraints in position, full width at half maximum and relative area of the satellite peaks. These values are available in [27]. The detailed decomposition spectrum is proposed in Fig. 3 with the assignment of the main peaks. For sake of clarity, satellite peaks are not assigned in the figure. For all the catalyst samples the same procedure was

Table 2
Binding energies (eV) measured by XPS for cobalt, molybdenum and sulfur species present at the surface of the CoMoP-S catalysts

	Co $2p_{3/2}$			Mo $3d_{5/2}$			S $2p_{3/2}$
	CoMoS	Co_9S_8	Co^{2+}	MoS_2	Mo^{5+}	Mo^{6+}	S^{2-}
CoMoP(0.1)-S	778.7	778.2	781.5	228.9	230.1	232.0	161.8
CoMoP(0.2)-S	778.7	778.1	781.3	228.8	230.1	232.0	161.6
CoMoP(0.3)-S	778.6	778.1	781.4	228.8	230.1	232.0	161.6
CoMoP(0.4)-S	778.6	778.1	781.4	228.7	230.1	232.1	161.5
CoMoP(0.5)-S	778.7	778.2	781.4	228.7	230.1	232.2	161.5
CoMoP(0.6)-S	778.6	778.1	781.4	228.7	230.0	232.0	161.5
CoMoP(0.7)-S	778.6	778.1	781.4	228.65	229.9	232.0	161.5
Mean value	778.6 ±0.1	778.1 ±0.1	781.4 ±0.1	228.8 ±0.1	230.0 ±0.1	232.0 ±0.1	161.6 ±0.1
Co-S	–	778.2	781.5	–	–	–	161.5
MoP-S	–	–	–	228.8	229.7	232.0	161.7

applied and conducted to the presence of Co(II) in an oxide environment, CoMoS and also Co_9S_8 phase at the respective binding energies 781.4–778.6 eV and 778.1 eV. The evolution of their concentration relatively to Co/Mo ratio will be discussed in Section 3.1.4.

3.1.3. S-species in CoMo(0.3)P-S

The S 2p spectrum obtained for the CoMo(0.3)P-S catalyst is presented in Fig. 4. The S 2p signal is composed of a main transition S $2p_{3/2}$ associated with a doublet S $2p_{1/2}$ which position, intensity and full width at half maximum were determined with a pure MoS_2 sample. On supported samples, the decomposition shows the presence of two different chemical species attributed for the lower binding energy at 161.6 eV to S^{2-} environment in association with Mo and Co to form MoS_2 and Co_9S_8, respectively, even if we cannot exclude the presence of terminal S_2^{2-} ligands at the same position as shown with model compounds [4,32]. The sulfur contribution at higher binding energy can traduce the presence of S_2^{2-} bridging ligands [4,32] or SH bond [28–30]. We relate it to the presence of Mo^{5+} species to form oxysulfide MoO_xS_y compounds. The processing parameters used to decompose the spectral envelopes from appropriate references (MoP, MoP-S and pure MoS_2 solid) are described in Table 3.

Thanks to the experimental decomposition, Table 4 reports the binding energy differences characteristic of the CoMoS phase between the main Co $2p_{3/2}$, Mo $3d_{5/2}$ and S $2p_{3/2}$ transitions. These values are specific of the CoMoS phase and different from the Co_9S_8 specie as already observed in the literature [1,2].

3.1.4. Quantification of the CoMoS and MoS_2 phases

The different amounts of cobalt do not influence the sulfurability of molybdenum (Fig. 5). About 80% of initial Mo is sulfided into MoS_2 whereas about 10% are still under their oxide form and 10% are defined as oxysulfided MoO_xS_y at an intermediate oxidation state.

In the case of the cobalt species, since the cobalt content deposited on alumina during the preparation of catalysts varies,

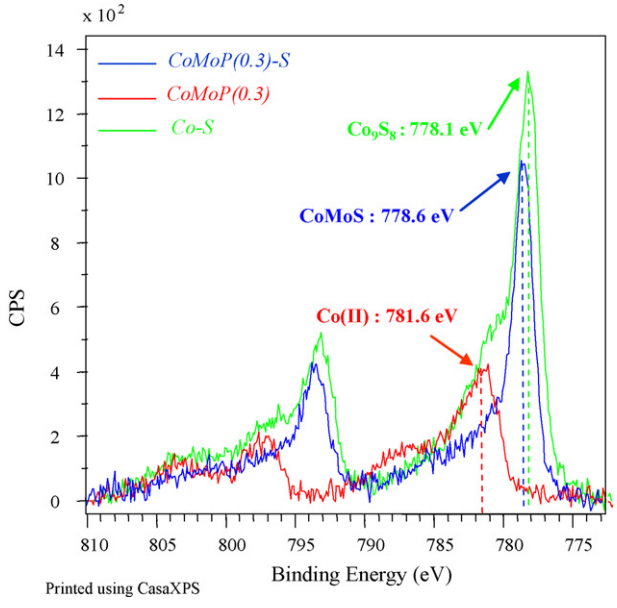

Fig. 2. Co 2p XPS spectra of CoMoP(0.3) (red), CoMoP(0.3)-S (blue) and Co-S (green). (For interpretation of the references to color in this figure legend, the reader is referred to the web version of the article.)

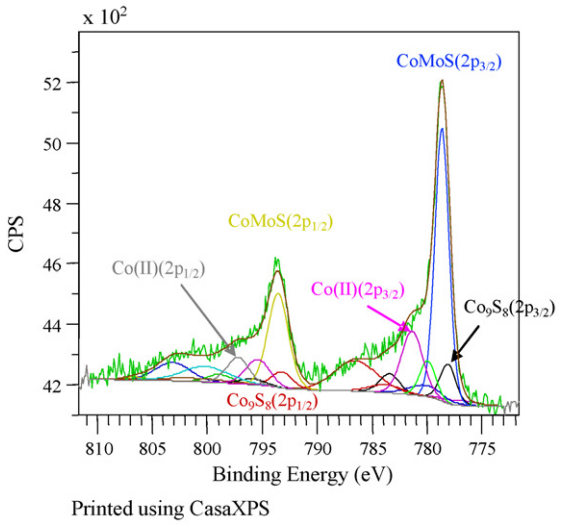

Fig. 3. Final decomposition of Co 2p XPS spectra for CoMoP(0.3)-S catalyst.

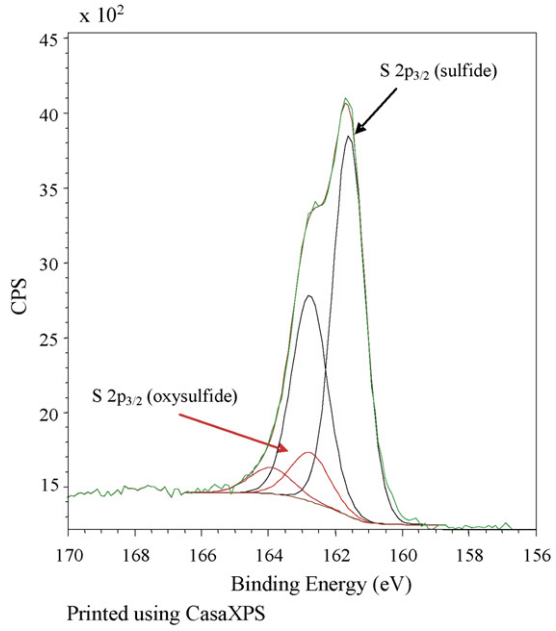

Fig. 4. Decomposition of S 2p XPS spectra for CoMoP(0.3)-S catalyst.

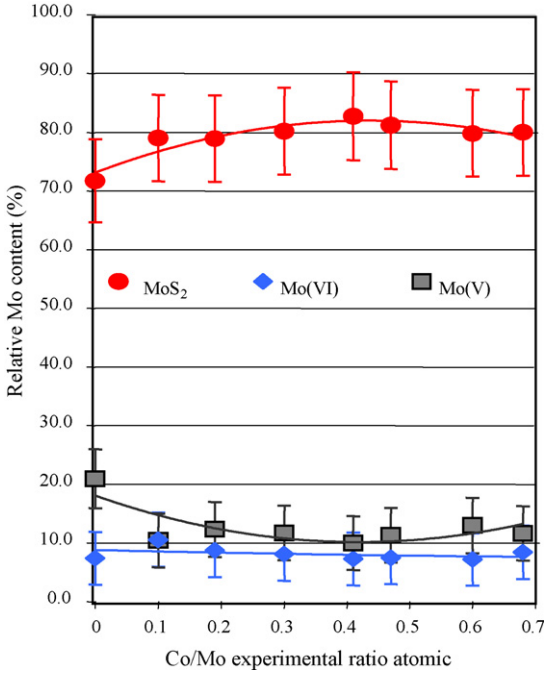

Fig. 5. Evolution of relative Mo species according to Co/Mo ratio.

it is initially preferable to follow the evolution of the contents expressed as a relative percentage in order to compare the proportions of each species detected at the surface of the samples. Fig. 6 depicts the evolution of the relative contents of the cobalt species, Co(II), Co_9S_8 sulfide and the mixed phase CoMoS, as a function of the atomic ratio Co/Mo (determined by X-ray fluorescence) for the CoMoP/Al_2O_3 catalysts. Contrary to the results obtained in the case of molybdenum, the atomic Co/Mo clearly influences the evolution of the cobalt species contents.

- For Co/Mo $\leq$0.5, the proportion of cobalt engaged in the mixed phase CoMoS is stable whatever the Co/Mo ratio, the proportion of residual Co(II) decreases slightly whereas the proportion of sulfide Co_9S_8 cobalt increases gradually with the Co/Mo ratio. It is important to highlight that when the maximum proportion of CoMoS phase is reached, only 60% of the cobalt atoms are engaged within this mixed phase.
- For Co/Mo >0.5, the results show a clear decrease of the proportion of CoMoS phase at the profit of the Co_9S_8 phase meaning that the additional cobalt added to reach the Co/Mo ratios of 0.6 and 0.7 does not allow to form more CoMoS phase, but is transformed into Co_9S_8. The proportion of residual Co(II) oxide is stable around 30% relative meaning that a non-negligible part of Co is difficult to sulfide.

Table 3
XPS processing parameters used to describe the sulfur phases contributions

Contribution	Binding energy (±0.10 eV)	Peak area	FWHM (±0.10 eV)
S^{2-} $2p_{3/2}$	161.60 (*A*)	*C*	1.13[a] (*E*)
S^{2-} $2p_{1/2}$	*A* + 1.18	*C* × 0.68	*E* × 1.11
S_2^{2-} $2p_{3/2}$	162.75 (*B*)	*D*	*E* × 1.20
S_2^{2-} $2p_{1/2}$	*B* + 1.18	*D* × 0.68	*E* × 1.32

[a] FWHM referenced to the FWHM of Al 2p peak, with a S/Al ratio of 0.68.

Table 4
Binding energy differences for the CoMoS and Co_9S_8 phases

Core levels transition	ΔBE (eV)
Co 2p-Mo 3d in CoMoS	549.8
Mo 3d-S 2p in CoMoS	67.2
Co 2p-S 2p in CoMoS	617.1
Co 2p-S 2p in Co_9S_8	616.5

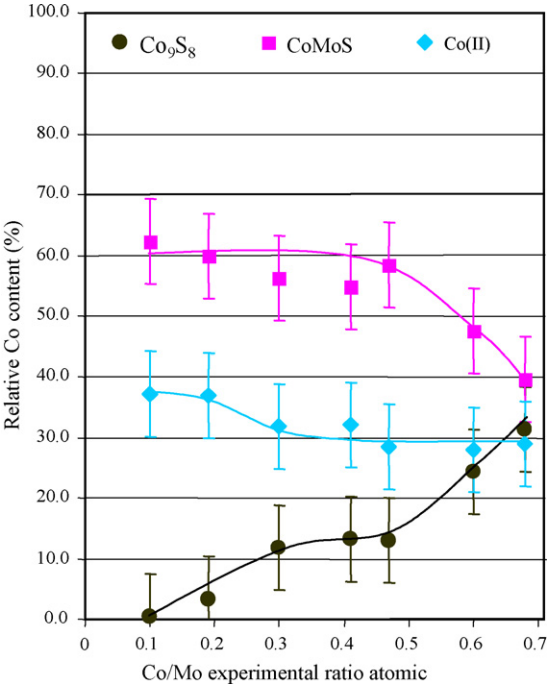

Fig. 6. Evolution of the relative content of the cobalt species according to the atomic ratio Co/Mo for the sulfided CoMoP(*X*)-S/Al_2O_3 catalysts.

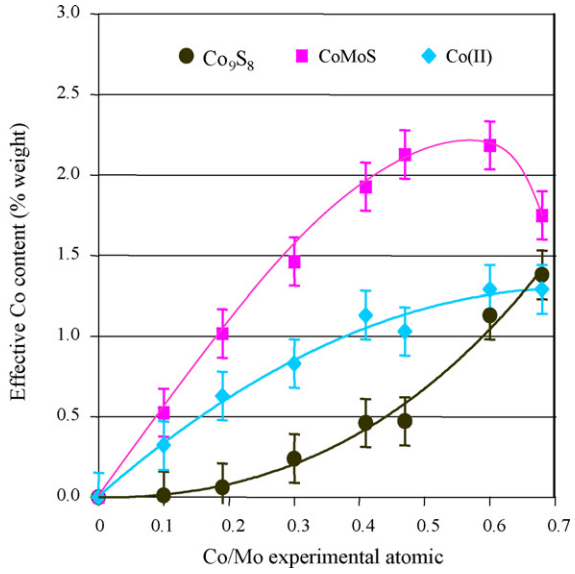

Fig. 7. Evolution of the effective content of the cobalt species to the atomic Co/Mo ratio for the sulfided CoMoP(*X*)-S/Al_2O_3 catalysts.

Fig. 7 plots the evolution of the effective contents of the cobalt species, expressed in weight percent, as a function of the Co/Mo ratio (determined by X-ray fluorescence). These results confirm the tendencies observed for the evolution of the relative contents for each cobalt species: for Co/Mo ratio up to 0.5, the quantity of CoMoS phase formed during sulfidation increases with the quantity of cobalt introduced in the catalyst. Nevertheless, a part of cobalt is sulfided into Co_9S_8 and there also remains a residual non-sulfided oxide phase. For Co/Mo ratio of 0.6 and 0.7, whereas the precursor oxide contains even more Co, the quantity of the CoMoS phase remains constant or decreases with respect to the Co_9S_8 species. The quantity of cobalt is thus "lost" in the form of Co_9S_8 and not engaged in the mixed CoMoS phase.

3.2. DFT calculations

3.2.1. Morphology models and promoter content

As explained in Section 2, the morphologies of the promoted CoMoS system for various Co content and reaction conditions have been investigated in details by Krebs et al. [16]. In the present paper, we focus on three possible models of morphologies with the corresponding edge local structures found in [16].

At a chemical potential of sulfur corresponding to HDT and sulfidation conditions used in the experimental part ($\Delta\mu_S = -0.87$ eV), the M-edge fraction is close to 0.5. The stable morphology models (close to a perfect hexagon) are represented in Fig. 8(a and b) for an average particles size of 33 Å given by the TEM analysis. As shown in [16], the Co content is always close to 100% at the S-edge due to the high stabilization of the edge energy in presence of Co. The S-coverage is 50% corresponding to a tetrahedral environment for Co. As discussed in [11,15], the Co–Mo distances calculated for such environment agree well with the earlier EXAFS characterizations [33–35]. At the M-edge, two competing edge structures may exist. The first configuration represented in Fig. 8(a) corresponds to the case where the M-edge is non-promoted (full segregation of Co from this edge). In this case, the Co/Mo ratio is close to 0.20 for the TEM particles size distribution. Mixed Co–Mo sites are present at the corners of the CoMoS particles: the Co atom belongs to the S-edge and the Mo atom to the M-edge. The maximal number of such mixed sites is thus 6 (one at each corner). The second stable configuration (Fig. 8(b)) corresponds to the partial decoration of the M-edge by Co (i.e. 50% Co). In this case, supplementary mixed Co–Mo sites belong to the M-edge and the maximal number of mixed Co–Mo sites is 9. As depicted in Refs. [14,16], Co atoms at the M-edge are in a square planar environment and have two Mo neighbors on the M-edge. Again, the Co–Mo distances calculated for such environment agree well with the earlier EXAFS characterizations [33–35]. As shown in [16], the energy of the configuration with Co pairing at the M-edge (Co–Co–Mo–Mo) is close to the alternated configuration (Co–Mo–Co–Mo represented in Fig. 8(b)). Such Co pairing at the M-edge would also be in line with recent interpretation of magnetic susceptibility measurements and NO adsorption [36]. The Co/Mo atomic ratio is 0.30 for the crystallite's model reported in Fig. 8(a). If we consider the particles size distributions given by TEM for the CoMoP(0.3)-S catalyst, and assume that promoted particles with different sizes are deduced from an homothetic transformation of the model of Fig. 8(a), the average Co/Mo ratio calculated over all particles is 0.33.

A third model may be relevant under specific sulfo-reductive conditions or preparation conditions (higher promoter loading). According to [16], Co can also be stabilized with 100% at the M-edge and S-edge as represented in Fig. 8(c). In this case, the M-edge fraction varies from 0.66 to 0.45 and the Co/Mo ratio is 0.49 for a particle's size of 33 Å. As for the previous models, the calculated average Co/Mo ratio over particle's size distribution is 0.51 for the CoMoP(0.5)-S catalysts. As explained in [16], the S-coverage at the edges represented in Fig. 8(c) is stable only for HDT reaction conditions ($\Delta\mu_S = -0.87$ eV), assuming that the metastable Co content (100%) at the M-edge remains unchanged. Such type of metastable model might exist, if the Co edge content and the morphology are assumed to be fixed at the preparation steps and remain unchanged in reaction conditions due to kinetic limitations. The S-coverage at the edges would vary due to exchange with H_2 and H_2S in the gas phase.

3.2.2. Core level shift

The values of 2p Co core level shift (ECLS) obtained by DFT calculations within the initial and final state approximations as described in the Methods are reported in Table 5. First, we notice that both approximations (initial and final states) give a positive value of the core level shift for Co atom located at the two edges with respect to Co in Co_9S_8 bulk. These trends are thus in agreement with the experimental results reported by XPS in the previous section or in earlier works [2]. The screening effect of the valence electron is thus negative and the final state approximation improves the core level shift value

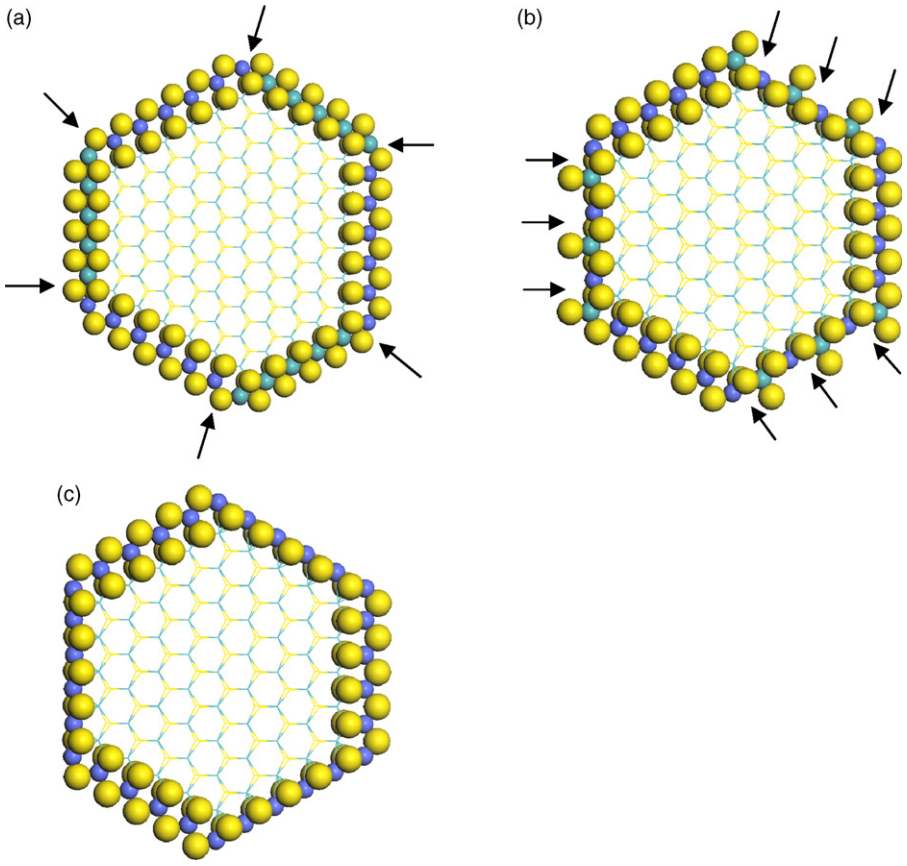

Fig. 8. The three possible models for the CoMoS nano-crystallites morphologies for TEM average size of 33 Å: (a) non-promoted M-edge (0% Co) and fully promoted S-edge (100% Co) in HDT conditions: Co/Mo = 0.16 and 6 mixed sites at corners (represented by arrows), (b) partially promoted M-edge (50% Co) and fully promoted S-edge (100% Co) in HDT conditions: Co/Mo = 0.30 and 9 mixed Co–Mo sites at corners and M-edges (represented by arrows), and (c) pure Co sites (100% Co atoms) on the M- and S-edge: Co/Mo = 0.49 and no mixed sites. This corresponds to a metastable state (see text for details).

when compared with experiments. The experimental accuracy depends also on the great variety of cobalt species: sulfides phases (Co_9S_8, CoMoS) and Co oxides as explained in the previous sections. In addition, it is known that the accuracy of the theoretical method is also within the range of ±0.1 eV for ideal metallic system [26]. As a consequence, we can consider that the final state approximation leads to reasonable results confirming that stronger binding energy of Co in CoMoS than in Co_9S_8 is a signature of the mixed phase even if a slight overestimate is observed. In addition, our calculations reveal a new interesting feature: the ECLS values depend on the type of edge. In particular, the ECLS value at the S-edge is higher than the value at the M-edge. A more detailed discussion of these trends will be the subject of a forthcoming paper [37].

Table 5
2p Co core level shift (ECLS see text for definition) in CoMoS with respect to the Co_9S_8 bulk phase reference within the initial state and final state approximations

Co site	Co-environment	Initial state	Final state
Co_9S_8	Octahedral (1/9); tetrahedral (8/9)	Reference	Reference
M-edge in CoMoS	Square planar	+1.21	+1.00
S-edge in CoMoS	Tetrahedral	+1.68	+1.51

4. Discussion

4.1. Co/Mo ratio: XPS and DFT insights

If we combine the XPS quantification of the CoMoS active phase and the DFT morphologies, it is now possible to propose a coherent model for the CoMoS nano-crystallites. The XPS quantification of the Co/Mo ratio in the nano-crystallites (Table 6) shows that the maximal proportion of the Co/Mo ratio does not exceed 0.47. Below that ratio, 60% of the Co atoms are present in the CoMoS phase. The remaining part is either as Co(II) species and a minor part in the Co_9S_8 phase. Increasing

Table 6
Mean Co/Mo atomic ratio in the crystallite as determined by XPS

Catalyst code	$(Co/Mo)^{a}_{slab}$
CoMoP(0.1)-S	0.1
CoMoP(0.2)-S	0.21
CoMoP(0.3)-S	0.30
CoMoP(0.4)-S	0.38
CoMoP(0.5)-S	0.45
CoMoP(0.6)-S	0.47
CoMoP(0.7)-S	0.39

[a] $(Co/Mo)_{slab}$ is calculated using CoMoS and MoS_2 quantification results from XPS experiments.

the Co/Mo ratio introduced at the impregnation step does not induce an increase of the CoMoS phase. In contrast, the proportion of the Co_9S_8 phase is increased (Fig. 6). According to this estimation, it is deduced that the upper limit of the Co/Mo ratio inside the CoMoS phase is close to 0.5.

Considering the TEM average particles size, for CoMoP(*X*)-S catalysts with $X \leq 0.3$, and according to the sulfidation conditions corresponding to $\Delta\mu_S = -0.87$ eV, the equilibrium morphology models correspond to Fig. 8(a or b). As explained in Section 3.2, the intrinsic Co/Mo ratio of the model of a promoted particle is comprised between 0.20 and 0.30. The resulting average Co/Mo ratios, calculated over particles distribution and assuming that all promoted particles are similar to those represented in Fig. 8(a or b), are also within this range. These values are very close to the one obtained by XPS for CoMoP(0.2)-S and CoMoP(0.3)-S. As a consequence, mixed Co–Mo sites (represented by arrows in Fig. 8(a and b) are present on both types of particles. The particle represented in Fig. 8(b) maximizes the number of mixed Co–Mo sites. It is also important to notice that the existence of such type of mixed sites has also been recently revealed by combining infrared spectroscopy and DFT calculations of CO adsorption on CoMoS [38].

For CoMoP(*X*)-S catalysts with $X \geq 0.4$, the XPS quantification of the Co species reveals intrinsic Co/Mo ratio greater than 0.3. This implies that a certain amount of promoted particles contain supplementary Co atoms at the M-edge. The maximal Co content at the M-edge would be represented by the model of Fig. 8(c). As calculated in Section 3.2, the mean Co/Mo ratio is 0.51 for the particle distribution of a CoMoP(0.5)-S catalyst if one assumes 100% Co at the M-edge. Since the Co/Mo ratio quantified by XPS is comprised between 0.38 and 0.47 (thus strictly lower than 0.51), we suggest that some particles may exhibit M-edge with Co content being greater than 50% (and strictly inferior to the full substitution). In this case, the number of mixed sites decrease significantly as shown by Fig. 8(c).

4.2. Impact on toluene-hydrogenation activity

The different CoMoP(*X*)-S catalysts were tested in toluene-hydrogenation and following simultaneously cyclohexane isomerisation (not reported here) which is constant whatever the Co/Mo ratio and has no influence on the hydrogenation activity. The hydrogenation activity (when normalized per mole of molybdenum) increases linearly with the atomic Co/Mo ratio from 0 to 0.3 (Fig. 9). For Co/Mo ratio higher than 0.3, the hydrogenation activity per mole of Mo remains constant. Increasing the Co loading for the same Mo loading does not improve the activity. After correcting the intrinsic activity due to non-promoted MoS_2 crystallites (0.37 mol/mol MoS_2/h) calculated from MoP-S catalyst (Fig. 9) taking into account that about 73% of initial Mo is sulfided (Fig. 5), we can plot the activity normalized by mole of Co atoms involved in the CoMoS phase (quantified by XPS) as a function of the amount of Co/Mo ratio (Fig. 10). Up to a Co/Mo atomic ratio of 0.3, the proportion of CoMoS phase increases while the monometallic

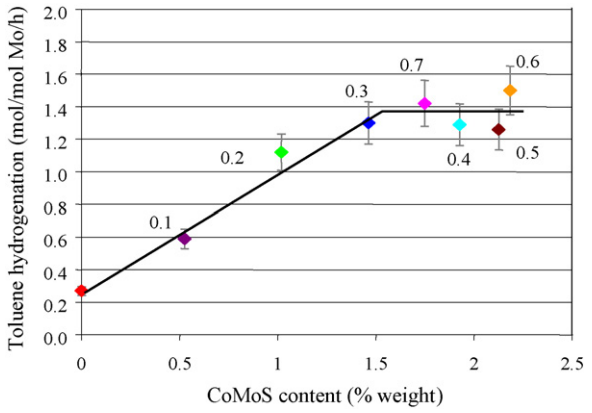

Fig. 9. Toluene-hydrogenation activity (per mole of Mo) as a function of the effective CoMoS amount quantified by XPS for the MoP-S and CoMoP(X)-S catalysts.

cobalt sulfur is low, the activity per site of active CoMoS phase is stable about 9.5 mol toluene-hydrogenated per mol CoMoS. In Fig. 10, we evidence that for Co/Mo = 0.1, 0.2 and 0.3 (region named A), the intrinsic activity (when normalized per Co edge site) remains high. For these ratios, the best model representing the average particle's morphology is given by Fig. 8(a and b) where two kinds of CoMoS sites exist on the crystallite: pure Co site at the S-edge, and mixed Co–Mo sites either at the corner or at the M-edge. In this domain denoted A in Fig. 10, the addition of Co in the catalysts leads to an increase of the proportion of promoted crystallites of the same type as represented in Fig. 8(b) compared to non-promoted ones, which explains the increase of the mean $(Co/Mo)_{slab}$ values obtained by XPS from 0.1 to 0.3 (Table 6).

For Co/Mo ratios greater than 0.4 (region named B), there is an increase of both CoMoS and Co_9S_8 species, however the intrinsic activity of CoMoS sites is significantly smaller (about two times). From the $(Co/Mo)_{slab}$ values and as the MET average size are the same as for the other catalysts, we propose that in this domain the supplementary cobalt increases the

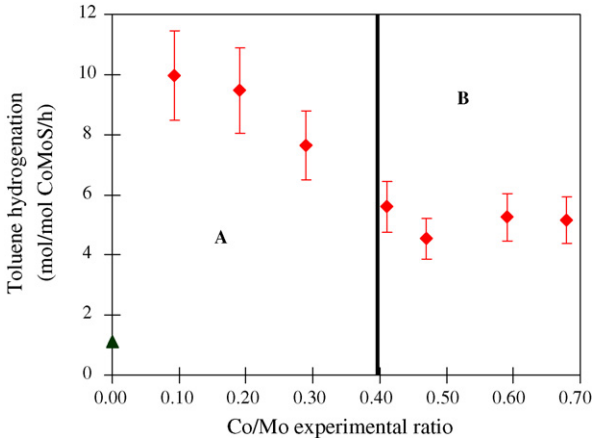

Fig. 10. Toluene-hydrogenation activity normalized per mol of Co atoms involved in the CoMoS active phase as quantified by XPS. (▲) is the activity of the non-promoted MoP-S catalyst (normalized per Mo-edge atoms for TEM size of 32 Å). Region (A): high activity in toluene-hydrogenation, region (B): low activity.

content at the M-edge of the crystallites to a substitution rate close to 100% for the 0.5 ratio, keeping a quasi-hexagonal shaped particle as shown in Fig. 8(c). According to this model, two kinds of active sites coexist at the edges: Co sites on S-edge, Co sites at the M-edge. As a consequence, only a negligible contribution of mixed Co–Mo site is expected. The decrease in activity observed for Co/Mo ratio greater to 0.3 is thus attributed to the progressive substitution of Mo atoms on M-edge and consequently to the disappearance of Co–Mo mixed site on this edge. For Co/Mo $\geq$ 0.4, the activity remains constant due to the fact that the crystallite is almost fully decorated and the type of sites remain unchanged whatever the Co content.

For the higher cobalt contents, the crystallite edges are almost completely saturated and the decrease of quantitative CoMoS for 0.7 ratio is due to a lower amount of promoted crystallite, as indicated by the mean $(Co/Mo)_{slab}$ value of 0.39 for this point instead of 0.47 for a quasi-100% substitution of all the detected slabs. The Co atoms are then in competition to form a sulfided and non-active species as shown by the rapid increase of Co_9S_8 recorded by XPS.

As a consequence, the important insight is that the intrinsic activity (per Co atom) of the CoMoS crystallite is optimized for Co/Mo ratio around 0.3 which corresponds to the existence of mixed Co–Mo sites on the M-edge. Above this critical value, the intrinsic activity in toluene-hydrogenation diminishes induced by the loss of a certain amounts of mixed sites after substitution of Mo atoms by Co.

To understand the role of mixed sites at the M-edge, earlier DFT results characterizing the CoMoS edge sites and the impact of the presence of Co on the sulfur–metal bond energy are relevant [11,39]. It was shown in Ref. [11] that the sulfur–metal bond energy at the M-edge decreases with the increase of the Co content on this edge. The stronger sulfur–metal bond energy (S–Mo) is obtained for the non-promoted active phase and the weaker (S–Co) for the M-edge with 100% Co. Mixed Co–Mo sites present at the M-edge exhibit intermediate sulfur–metal bond energy values comprised between non-promoted Mo-site and pure Co site. Recent microkinetic investigations of the toluene-hydrogenation on various sulfide catalysts have shown that a volcano curve correlates well the intrinsic activities of the sulfides with their sulfur–metal bond energies [40,41]. Intermediate sulfur–metal bond energies of mixed Co–Mo sites provide the optimal situation in terms of surface concentrations for the different species involved in the kinetically limiting step: especially –SH groups and toluene. These kinetic results and the present study explain why a full saturation of the M-edge by Co leads to a decrease of the toluene-hydrogenation intrinsic activity. In contrast, the mixed Co–Mo sites at the M-edge appear thus crucial for providing the optimal intermediate sulfur–metal bond energy required for ensuring an optimal edge concentration of reactive species involved in toluene-hydrogenation.

To explore further the role of mixed sites, we have simulated at the DFT level the first adsorption step of toluene on the Co promoted S-edge and M-edge. At the promoted S-edge no stable toluene adsorption is stable, due to the repulsive interaction of the unpaired electrons of S-bridging atoms in the tetrahedral environment of the Co with the π-electrons of the toluene ring. In contrast, the promoted M-edge with mixed Co–Mo sites (in an alternated position) provides a stable configuration as the one represented in Fig. 11. The neighbouring –SH and –H species offer a favorable situation for the subsequent hydrogenation steps of toluene in a consistent way as proposed in the kinetic modeling [40,41].

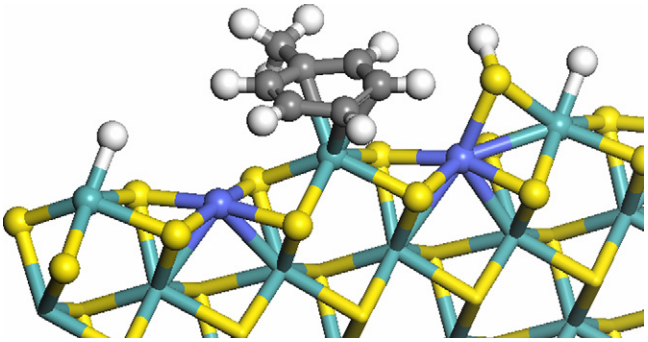

Fig. 11. DFT optimized local structure of toluene adsorption on the Co–Mo mixed sites at the M-edge in presence of –SH and –H species.

5. Conclusions

Using a multitechnique approach, this paper has investigated the properties of the CoMoS active phase combining TEM, XPS and DFT calculations. TEM has shown that the mean particle size close to 33 Å does not depend on the Co content. XPS quantification of the Mo species has shown that 80% of the Mo species are present in the sulfided MoS_2 phase. The binding energy of the 2p core electrons of Co has been found +0.55 eV higher than the Co_9S_8 reference phase. The DFT calculation of the core level shift of Co at the edges of the CoMoS with respect to Co_9S_8 has confirmed the increase of binding energy within the final state approximation. This positive core level shift can be seen as a signature of the CoMoS phase. In addition, the calculated core level shift is found higher on the S-edge than on the M-edge.

The decomposition of the XPS spectrum has enabled a precise quantification of the Co species engaged in the CoMoS phase. Combining the XPS quantification with the DFT morphology models of the CoMoS crystallite has revealed the existence of mixed Co–Mo sites at the M-edge for Co/Mo atomic ratio of 0.3. This ratio has been found to be optimal for providing the higher intrinsic activity in toluene-hydrogenation. Above this ratio, the further addition of Co at the M-edge decreases the intrinsic catalytic activity in toluene-hydrogenation (when normalized per Co edge site). The decrease of the amount of mixed Co–Mo sites at the M-edge has been attributed to this loss of intrinsic activity for Co/Mo ratio greater than 0.3. In line with the volcano curve's concept, the intermediate sulfur–metal bond energy provided by mixed Co–Mo sites at the M-edge is proposed to explain the optimal promoter edge content found for Co/Mo close to 0.3.

Reference

[1] M. Breysse, B.A. Bennet, D. Chadwick, M. Vrinat, Bull. Soc. Chim. Belg. 90 (1981) 1271.
[2] I. Alstrup, I. Chorkendorff, R. Candia, B.S. Clausen, H. Topsoe, J. Catal. 77 (1982) 397.
[3] A.D. Gandubert, C. Legens, D. Guillaume, S. Rebours, E. Payen, Surf. Interface Anal. 28 (2006) 206.
[4] L. Coulier, V.H.J. de Beer, J.A.R. van Veen, J.W. Niemantsverdriet, Top. Catal. 13 (2000) 99.
[5] F.B. Garreau, H. Toulhoat, S. Kasztelan, R. Paulus, Polyhedron 5 (1986) 211.
[6] S. Houssenbay, S. Kasztelan, H. Toulhoat, J.P. Bonnelle, J. Grimblot, J. Phys. Chem. 93 (1989) 7176.
[7] L. Coulier, V.H.J. de Beer, J.A.R. van Veen, J.W. Niemantsverdriet, J. Catal. 197 (2001) 26.
[8] A.D. Gandubert, C. Legens, D. Guillaume, S. Rebours, E. Payen, Oil Gas Sci. Technol. - Rev. IFP 62 (2007) 79.
[9] P. Raybaud, Appl. Catal. A: Gen. 322 (2007) 76.
[10] L.S. Byskov, J.K. Norskov, B.S. Clausen, H. Topsoe, Catal. Lett. 64 (2000) 95.
[11] P. Raybaud, J. Hafner, G. Kresse, S. Kasztelan, H. Toulhoat, J. Catal. 190 (2000) 128.
[12] A. Travert, H. Nakamura, R.A. van Santen, S. Cristol, J.F. Paul, E. Payen, J. Am. Chem. Soc. 124 (2002) 7084.
[13] S. Kasztelan, H. Toulhoat, J. Grimblot, J.P. Bonnelle, Appl. Catal. A: Gen. 13 (1984) 127.
[14] H. Schweiger, P. Raybaud, G. Kresse, H. Toulhoat, J. Catal. 207 (2002) 76.
[15] H. Schweiger, P. Raybaud, H. Toulhoat, J. Catal. 212 (2002) 33.
[16] E. Krebs, B. Silvi, P. Raybaud, Catal. Today 130 (2007) 160.
[17] P. Blanchard, A. Griboval, E. Payen, M. Fournier, J.L. Dubois, Catal. Today 45 (1998) 277.
[18] J.P. Perdew, Y. Wang, Phys. Rev. B 45 (1992) 13244.
[19] J.P. Perdew, J.A. Chevary, S.H. Vosko, K.A. Jackson, M.R. Pederson, D.J. Singh, C. Fiolhais, Phys. Rev. B 46 (1992) 6671.
[20] W. Kohn, L.J. Sham, Phys. Rev. A 140 (1965) 1133.
[21] G. Kresse, D. Joubert, Phys. Rev. B 59 (1999) 1758.
[22] T. Koopman, Physica 1 (1993) 104.
[23] B. Johansson, N. Martensson, Phys. Rev. B 21 (1980) 4427.
[24] L. Köhler, G. Kresse, Phys. Rev. B 70 (2004) 165405.
[25] J.F. Janak, Phys. Rev. B 18 (1978) 7165.
[26] S. Lizzit, A. Baraldi, A. Groso, K. Reuter, M.V. Ganduglia-Pirovano, C. Stampfl, M. Scheffler, Phys. Rev. B 63 (2001) 205419.
[27] A.D. Gandubert, C. Legens, D. Guillaume, E. Payen, Surf. Interf. Anal. 38 (2006) 206.
[28] A. Galtayries, S. Wisniewski, J. Grimblot, J. Electron Spectros. Related Phenomena 87 (1997) 31.
[29] A.M. Venezia, Catal. Today 77 (2003) 359.
[30] J.C. Dupin, D. Gonbeau, I. Martin-Litas, Ph. Vinatier, A. Levasseur, Appl. Surf. Sci. 173 (2001) 140.
[31] M.W.J. Craje, S.P.A. Louwers, V.H.J. de Beer, R. Prins, A.M. van der Krann, J. Phys. Chem. 96 (1992) 5445.
[32] Th. Weber, J.C. Muijsers, J.W. Niemantsverdriet, J. Phys. Chem. 99 (1995) 9194.
[33] H. Topsøe, B.S. Clausen, N.-Y. Topsøe, K.J. Pedersen, W. Niemann, A. Müller, H. Bögge, B. Lengeler, J. Chem. Soc., Faraday Trans. I 83 (1987) 2157.
[34] S.M.A.M. Bouwens, R. Prins, V.H.J. de Beer, D.C. Koningsberger, J. Phys. Chem. 94 (1990) 3711.
[35] S.M.A.M. Bouwens, J.A.R. van Veen, D.C. Koningsberger, V.H.J. de Beer, R. Prins, J. Phys. Chem. 95 (1991) 123.
[36] Y. Okamoto, M. Kawano, T. Kawabata, T. Kubota, I. Hiromitsu, J. Phys. Chem. B 109 (2005) 288.
[37] D. Costa, E. Krebs, M. Breysse, P. Raybaud, H. Toulhoat, in preparation.
[38] A. Travert, C. Dujardin, F. Maugé, E. Veilly, S. Cristol, J.-F. Paul, E. Payen, J. Phys. Chem. B 110 (2006) 1261–1270.
[39] H. Toulhoat, P. Raybaud, J. Catal. 216 (2003) 63.
[40] N. Guernalec, T. Cseri, P. Raybaud, C. Geantet, M. Vrinat, Catal. Today 98 (2004) 61.
[41] N. Guernalec, C. Geantet, P. Raybaud, T. Cseri, M. Aouine, M. Vrinat, Oil Gas Sci. Technol.—Rev. IFP 61 (2006) 515.